RSC Advances

ROYAL SOCIETY OF CHEMISTRY

www.rsc.org/advances

Hybrid tapered silicon nanowire/PEDOT: PSS solar cells

Xiu Gong, Yurong Jiang, * Meng Li, Hairui Liu, and Heng Ma, *

College of Physics & Electrics Engineering, Henan Normal University, Henan Key Laboratory of Photovoltaic Materials, Xinxiang 453007, PR China

ABSTRACT:

A tapered silicon nanowires arrays (TSiNWs) / poly (3, 4-ethylenedioxythiophene)/poly (styrenesulfonate) (PEDOT: PSS) hybrid solar cell was gained based on alkali treatment processing. TSiNWs are engineered by combining electroless etching and alkali solution in which the morphology of the tapered nanowire can be controlled by changing the immersing time. The results show that the alkali treatment could taper the silicon nanowires so that the polymer could conformally infiltrate into SiNWs via spin-coating. The experiment results demonstrate that the length and morphology of SiNWs are key factors for improving the cell performance. Compared to the SiNWs/polymer hybird device, TSiNWs/polymer hybrid solar cell can achieve a high power conversion efficiency of 6.87% and short-circuit current density of 26.7mA/cm^2. Therefore, tapered silicon nanowires are promising structures for realizing economically viable hybrid solar cells based on very a simple, scalable, and low-cost solution route.

KEYWORDS: Hybird solar cell; Tapered Si nanowires; Alkali treatment; PEDOT: PSS

*Corresponding Author: E-mail: jiangyurong@whut.edu.cn(Yurong Jiang); hengma@henannu.edu.cn (Heng Ma).

Introduction

High-efficiency crystalline silicon (c-Si) has dominated photovoltaic industries for years due to its own advantages such as nontoxicity, high abundance material supply, and efficient separation of light-generated charge carriers.[1-5] However, photovoltaic industry based on c-Si with high crystallinity and purity has been limited because of expensive fabrication processes. For instance, the p-n junction of c-Si solar cells is normally formed by furnace diffusion at very high temperatures (~1000°C). Thus, there has been significant interest in fabricating devices at low temperatures.

Organic solar cells based on conjugated polymers have attracted much attention because of their solution processability and mechanical flexibility.[5, 6] However, the conversion efficiency (PCE) of organic solar cells is limited due to poor mobility of organic materials, which is lower in comparison with that of the Si-based devices. Therefore, hybrid solar cells based on Si and conjugated polymers combine both of their advantages at low temperatures provide a possible alternative technology to simplify fabrication processes and reduce the costs.[6-20] A conjugated polymer of poly (3, 4-ethylene dioxythiophene): poly-(styrenesulfonate) (PEDOT: PSS), which is transparent and conductive (<1000 S/cm) organic material, can be deposited by a solution-processed method to form a Schottky junction with Si.[10-13] Thus, the efficiency of the hybrid PEDOT: PSS/organic solar cell may be comparable to a conventional Si p-n junction solar cell in principle.

To reduce the cost of photovoltaic devices further, significant efforts have been made in reducing the thickness of the Si hybrid solar cells composed of Si substrate, which requires considerable improvement in light absorption. The nanoscale surface structures play leading roles in the for thin-film solar cells, which can enhance light absorption in comparison with traditional microscale texturing for crystalline Si solar cells.[14,15] Moreover, nanostructures not only exhibit an excellent light absorption capability by light antireflective and scattering effects but also offers the radial p-n junction architectures which provide a large junction area for charge separation.[1,2,5] The radial junction structures can decouple the light absorption and charge-carrier collection direction.[21-23] Therefore, radial p–n junction of silicon nanowires arrays (SiNWs) can provide an efficient charge transport and a high light harvesting capability.[23-25] The unique electrical and optical properties can potentially improve the cell efficiency and reduce the cell cost. Therefore, the development of hybrid solar cell composed with SiNWs/organic core/shell has become a kind of inevitable trend. Recently, hybrid solar cell of SiNWs/organic with power conversion efficiency (PCE) of 6%–11% has been achieved[26-29]. Many approaches have been used to improve the filling ratio of the organic solution in interior SiNWs such as changing density of SiNWs by PCl_5 solution treatment[13], fabricating Si nanocones by nanosphere lithography[29], obtaining regular SiNWs by template[6] and so

on. However, these approaches limit hybrid solar cell to realize industrialization in practice due to complicated manufacturing process, expensive template increase the fabrication cost, using toxic solution to treatment and against large-scale production. In addition, according to Rayleigh Scattering Laws, the enhancement of the scattering degree for some long wavelengths can cause a resonance Rayleigh scattering, which makes the backward scattering light unable to enter SiNWs internal.[29] This will lead to the reflectivity of long wavelength will be higher than that of short wavelength.

Therefore, using facile and effective method to further optimize antireflection and the morphology of nanoscale texturing of the hybrid solar cell is a necessary work for improving the performance of SiNWs-based hybrid devices. In this paper, we introduce a facile method to improve the photovoltaic performance based on TSiNWs by alkali chemical treatment, which can not only rise to efficient charge separation/transport but also can improve the spectral response and enhance the surface antireflection. The TSiNWs with the proper length allowed for conformal polymer surface coverage via spin coating to form a Si/organic core/shell nanowires arrays.

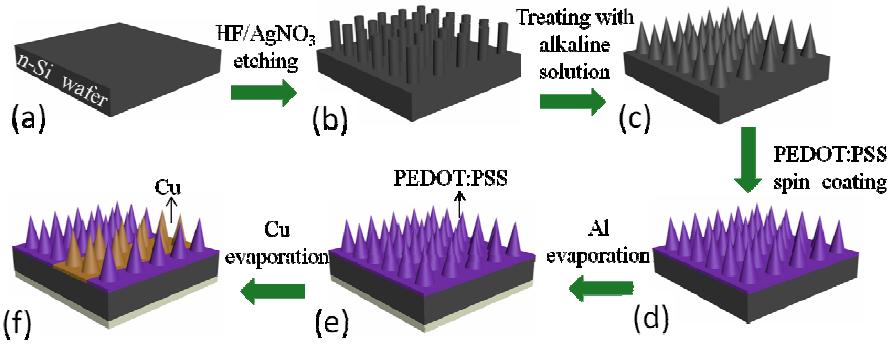

Fig. 1 Schematic illustration of the fabrication process for TSiNWs/PEDOT: PSS solar cells. (a) RCA clean of the n-type Si (100) wafer, (b) SiNWs array fabricated by metal assisted chemical etching process, (c) TSiNWs array fabricated by anisotropic etching technique using the alkaline solution, (d) after spin-coating of PEDOT:PSS, (e) after evaporating metal Al cathode, and (f) evaporating Cu film electrode with 12 nm thick as anode.

Experimental

SiNWs and TSiNWs fabrication

In the experiment, n-type Si (100) substrate with resistivity of 2~4 Ω cm was cut into 1.5 cm ×1.5 cm wafers. SiNWs were fabricated by metal-assisted electroless etching. TSiNWs are obtained by SiNWs immersing alkaline solution. First, n-type Si (100) substrates were ultrasonically vibrated in acetone and ethanol at room temperature for 10 min to remove the surface contaminations, respectively. Clean Si (100) wafer were immersed in a solution of 0.48-M hydrofluoric acid (HF) and 0.02-M silver nitride ($AgNO_3$) at room temperature. The lengths of the nanowires were fabricated by changing the etching time of 1,3,5,7 and 10min. After etching, the as-prepared

SiNWs were dipped into a HNO_3 for 20 min to remove the tree-like silver dendrites. After all the samples were rinsed with deionized (DI) water and soaked in HF solution to remove any oxide. To fabricate tapered shape on the top-ends of the nanowires using anisotropic etching in alkaline solution, the cleaned SiNWs array were immersed in 30wt% NaOH solution for various times at room temperature. Finally, TSiNWs were rinsed with the standard cleaning process for semiconductors and dried with nitrogen.

Hybrid Solar cell fabrication

PEDOT: PSS (Clevios PH500) mixed with 5wt% dimethyl sulphoxide (DMSO) and 1 wt% Triton X-100 (surfactant) solution was spin coated onto the SiNWs array substrate at 3000 rpm for 15s and 5000 rpm for 45s to form SiNWs/ PEDOT: PSS core−sheath radial heterojunction structure, and then the samples were thermal annealed at 140°C in a dry atmosphere for 10 min to remove the solvent. Following that, a 150nm thick aluminum was deposited on the backside of the Si substrates by thermal evaporation to form cathode contact. Finally, a 12 nm semi-transparent Cu layer (2mm × 2mm) was deposited on top of the PEDOT: PSS layer by thermal evaporation to form anode contact. Figure. 1 depicts the Schematic illustration of the fabrication process for a TSiNWs/PEDOT: PSS solar cells.

Characterization of SiNWs

Nanoscale surface and cross-sectional morphology of the SiNWs were characterized using a scanning electron microscopy (SEM SUPRA™ 4.0).The reflectivity of the substrates was measured by a UV-3600 spectrophotometer with an integrating sphere in the wavelength range of 300–1300nm. The external quantum efficiency (EQE) measurements were carried out by using a calibrated Newport 818-UV sensor and a monochromator (Acton Spectra Pro 2300i) with a lock-in amplifier (SR-830) and a SR540 optical chopper. The photovoltaic current density-voltage (J−V) characteristics of the solar cells were measured at air mass (AM) 1.5 G illumination. The surface wetability property between nanowires and PEFOT:PSS were measured by a contact angle apparatus.

Results and discussion

Organic hybrid structure

The structure of hybrid TSiNWs/PEDOT: PSS solar cell is shown in Fig. 1(f). TSiNWs are easy to make PEDOT: PSS infiltrate into the space between the Si nanostructures, and therefore to form a core (SiNWs)-shell (PEDOT: PSS) geometry. This core-shell structure can make the direction of the light absorption and hole (minority carrier) transport become orthogonal, which can allow a short minority diffusion length and modest charge carrier mobility and gave rise to an efficient charge separation/transport. The hole and electron are collected

by a Cu anode and an Al cathode, respectively.

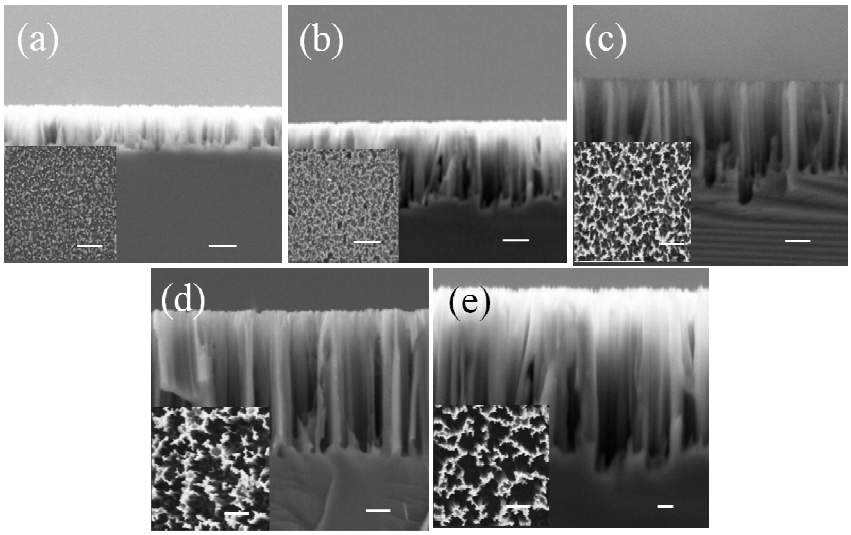

Fig. 2 Cross-section SEM images of SiNWs with the wire lengths of (a) 0.15μm, (b) 0.30 μm, (c) 0.45 μm, (d) 0.65 μm, and (e) 0.90 μm, respectively. The inset is the top view SEM of the SiNWs. All the scale bars are 100 nm.

Table 1. Solar cells performance of the hybrid solar cells fabricated from different SiNWs with the lengths of 0.15, 0.30, 0.45, 0.65, and 0.90 μm respectively.

SiNWs of Etching time (min)	Wire length (μm)	J_{sc} (mA/cm^2)	V_{oc} (V)	FF (%)	PCE (%)
1	0.15	13.08	0.429	50	2.84
3	0.30	16.52	0.433	51	3.32
5	0.45	20.59	0.435	51	4.58
7	0.65	14.84	0.421	50	3.27
10	0.90	12.08	0.417	47	2.67

Effect of SiNWs lengths on cell performance

The length of SiNWs, which is determined by the etching time in the mixing solution of HF and $AgNO_3$, plays an important role in device performance. SiNWs with average height of 0.15, 0.30, 0.45, 0.65 and 0.90 μm were fabricated by etching the sample for 1, 3, 5, 7, and 10 min. Fig. 2 shows the cross-sectional SEM images of the different lengths of SiNWs, the inset shows the corresponding morphologies of SiNWs coated with PEDOT: PSS. Five cells were fabricated for each value of the SiNWs length and their electrical performance was measured. Fig. 3(a) shows the current density-voltage (J-V) characteristics of the devices with different SiNWs lengths. All the characteristics parameters of the cells are summarized in table 1.

When increasing the length of SiNWs from 0.15μm to 0.90μm, the cell performance displays a peak shape.

The cell with the length of 0.45μm-SiNW/PEDOT: PSS possesses the highest short circuit current density (J_{sc}) of 20.13 mA cm^2 and highest open circuit voltage (V_{oc}) of 0.435 V, and therefore results in the largest power conversion efficiency (PCE) of 4.45% among the five cells. For other cells with shorter and longer SiNWs, their optoelectronic performance is poor. The reason is that the shorter SiNWs do not get enough effective area for the core (SiNWs)-shell (PEDOT: PSS) compared to the longer SiNWs. However, too long SiNWs itself are easy to form aggregation at the top to prevent the organic material going inside the space of SiNWs. Therefore, an appropriate length of SiNWs is important for the devices. For this reason, both too long and too short SiNWs cannot provide ideal environment for photon converting to electron. Similar effects have also been observed by Zhang [13] et al. and Chen [30] et al. In this work, the length of 0.45 μm SiNWs is a proper size.

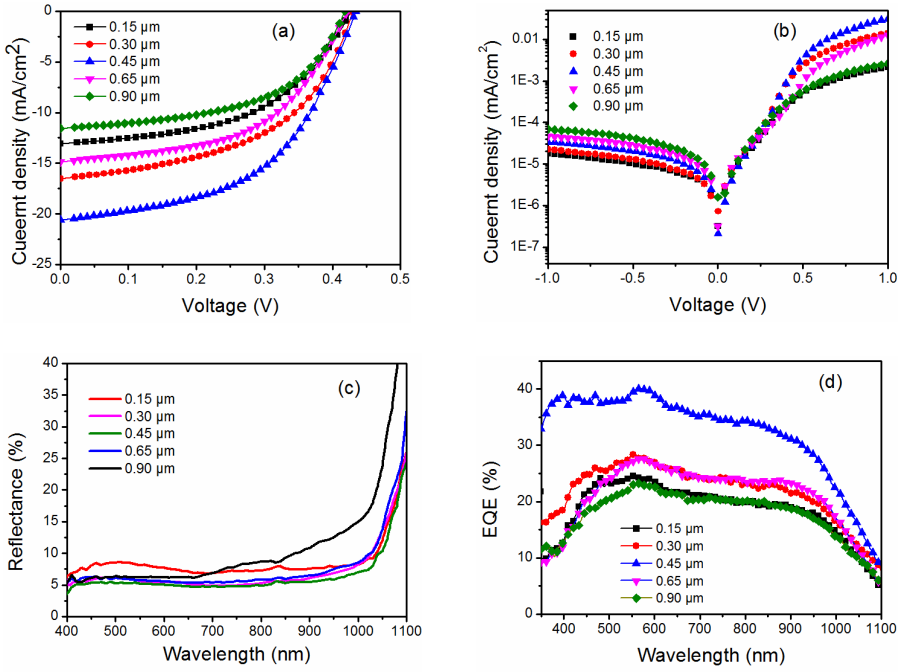

Fig. 3 (a) J–V (b) Dark current density-voltage (J-V) characteristics (c) Reflectance and (d)EQE spectra of the hybrid solar cells fabricated from different SiNWs with the lengths of 0.15, 0.30, 0.45, 0.65, and 0.90 μm, respectively.

In order to detail analysis the effect of SiNW lengths on the PCE, and then dark current density, light reflectance and external quantum efficiency of the cells were measured.

The dark current density of the cells shown in Fig. 3(b) is also reflected the fact that the larger aggregations of the longer SiNWs lead to more surface defect and a low separation efficiency of hole and electron, as discussed previously. On the contrary, the cells with shorter SiNWs express a small dark current density due to the organic PEDOT: PSS can cover SiNWs well to form a uniform core (SiNWs)–shell (PEDOT: PSS). This phenomenon has also been observed by other researchers. [13, 18, 31]

What's more, the dark J–V curves not only exhibit rectifying characteristics but it also demonstrate that the SiNWs/PEDOT:PSS heterojunctions behave as well-defined diodes. Therefore, we can calculate the ideality factor n of diode to further explain electrons and holes recombination degree at interface of variable length SiNWs / PEDOT:PSS, then we will discuss it in more detail. Using the thermionic emission theory, the dark J-V relation for heterojunction of the TSiNWs/PEDOT: PSS can be expressed as follows:

$$J = J_0\{\exp\left[\frac{q(V - IRs)}{nKT}\right] - 1\} \quad (1)$$

Where K is the Boltzmann, T is the absolute temperature in Kelvin, q is the unit charge of a single electron, n is the ideality factor, Rs is the series resistance of the diode and J_0 is the reverse bias saturation current represented. Ideality factor n is a measurement to describe the quality of p-n junction and complex type of the cell. For an ideal diode, n=1, which indicate the current transport mechanism in the diode conforms to pure thermionic emission. But for a non-ideal diode, n=2 indicate the current transport is dominated by electron-hole recombination current, especially in complex type strong cell. By rearranging the above equation, n is given by

$$n = \frac{q}{KT}\frac{dV}{d(\ln I)} \quad (2)$$

The values of n for the SiNWs/PEDOT: PSS heterojunction diodes can be calculated by using a method developed by Cheung et al[32], where ratio of dV/d(ln I) we can be generated from the forward J-V characteristics in Fig .3(b). Therefore, using this approach, the value of n corresponding to heterojunction of variable length SiNWs / PEDOT:PSS can be calculated from the forward J-V characteristics. After fitting the dark J–V data, the diode ideality factor and the reverse saturation current are estimated and exhibited in tables 2. The value of n increases as increasing the length of SiNWs, and the device with the 0.15 μm length of SiNWs displays the value of n and I_s are the smallest，which indicates SiNWs/PEDOT:PSS heterojunctions behave as well-defined diodes and smaller recombination rate of electrons and holes on the junction surface of P-N[13]. For the longer wires, with the length of SiNWs increasing, it is hard to make PEDOT:PSS wrap every wire up well; eventually lead to more surface defect and high recombination rate. However, the hybrid cell based on the 0.15μm length of SiNWs shows a modest PCE compared to the device with the 0.45 μm length of SiNWs. It should be ascribed to the high reflectivity of short SiNWs and the lower junction area.

Table 2. The diode ideality factor and the reverse bias saturation current of the hybrid device made from SiNWs with different wire lengths of 0.15μm, 0.30μm, 0.45μm, 0.65μm, 0.90μm, respectively.

Wire length	n	J_s (mA)
0.15μm	1.83	1.47×10^{-4}
0.30μm	2.03	3.11×10^{-4}
0.45μm	2.14	3.83×10^{-4}
0.65μm	2.58	6.45×10^{-3}
0.90μm	2.89	8.89×10^{-3}

The light reflectance behavior of SiNWs as a function of wavelength ranging from 400 nm to 1100 nm layer is shown in Fig. 3(c). With increasing the length of SiNWs, the reflectance of the device decreases progressively although the difference is slight. This antireflective effect may be easily explained by the enhanced light-trapping effect arising from the longer SiNWs[31].

To further understand the device's characteristics, the external quantum efficiency (EQE) as a function of spectra is illustrated in Fig. 3(d). The cell with 0.45μm-SiNWs /PEDOT: PSS shows the best EQE compared with others. For shorter length of $SiNW_S$, along with the stronger light reflectivity (see Fig. 3(c)), it also possesses smaller junction area; so the limited absorption light cannot provide enough PCE. For longer SiNWs, the larger aggregation on the top that prevents the organic material going into the root segment cannot from an effective junction area (in table 2). Meanwhile, the invalid aggregation domain does also absorb the incident light to convert heat not for carriers. As a result, EQE of the 0.45 μm SiNWs/PEDOT: PSS also confirms the above discussion, i.e. the reason is consistent.

Effect of alkali treatment SiNWs on cell performance

Although the device with 0.45μm-SiNWs/PEDOT: PSS with the etching for 5 minutes has the best performance compared to the others, the relative experiments have been proved at the previous reports.[8, 33] Besides the length of the SiNWs can influence the performance of the cell, the morphology of SiNWs is another important factor in determining the cell property. For a easily aggregation SiNWs, the polymer is suspended on the top part of SiNWs resulting in a poor infiltrating into the spaces of SiNWs which is disadvantageous of carrier transporting, resulting in the carrier high recombination and an inferior PCE.[6-8, 13, 16] In order to overcome this issue, to improve the interface between the polymer and Si, a further modifying surface of SiNWs structure is needed. In this study, a simple and effective method that SiNWs dips in NaOH solution is used to modify the nano structure[33-36].

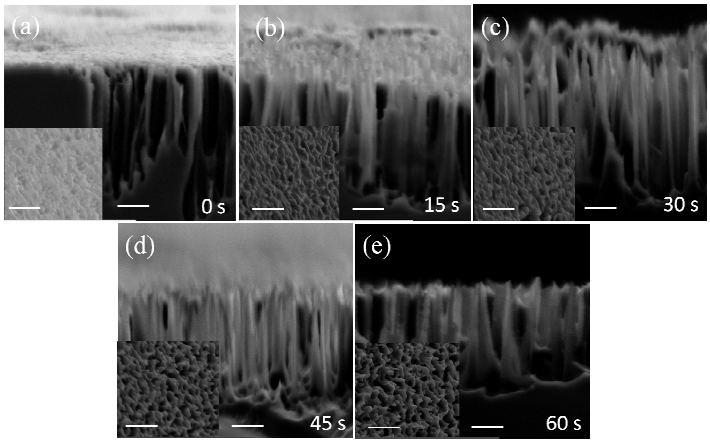

Fig. 4 Cross-section SEM images of 0.45μm SiNWs with 30wt% NaOH solution treatment for (a) 0 s, (b) 15 s, (c) 30 s, (d) 45 s and (e) 60 s, respectively. The inset is tilted-view (30°) SEM images of the different surface morphologies of SiNWs, all SiNWs coated with PEDOT: PSS, All the scale bars are 200 nm.

The different morphology of SiNWs shown in Fig. 4 can be obtained at the different 30wt%NaOH treating time. From cross-section SEM images Fig. 4 (a) to Fig. (e), one can find that SiNWs are changed into needle-like shape, and that the spacing between nanowires becomes also big gradually, here, it is named tapered shape silicon nanowires arrays (TSiNWs). In the figure 4, it can also be clearly observed that the PEDOT:PSS film is suspended on the surface of SiNWs, while the PEDOT:PSS film are gradually penetrated into interior of SiNWs with increase time of alkali treatment. In addition, corresponding inset in fig.4 shows that surface morphologies from smooth, subtle to stocky, similarly, the results prove that surface morphology of TSiNWs with 30s alkali treatment is more uniform than other morphology, and the length of wires is nearly invariable.

Generally, the smooth surface is difficult for PEDOT: PSS penetrating into the gaps of nanowires deeply and forming structure of Si/organic core/shell. Although the short nanowires are facile for PEDOT: PSS penetrating into the gaps, the effective junction area will be reduced (shown in fig 4(e)). Therefore, nanowires without alkali treatment are adverse organic solutions to form a more continuous layer on the wire.

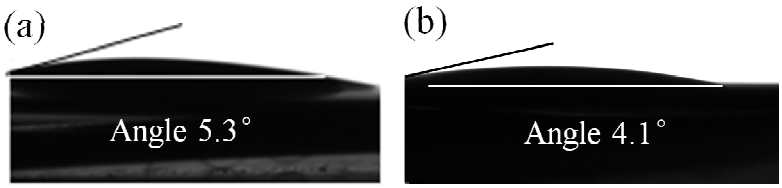

Fig.5 Photograph of the different surface wettability (a) SiNWs and (b) TSiNWs.

The wetability of SiNWs and TSiNWs were evaluated (see Fig.5(a), 5(b)), the results demonstrate that the change of the contact angle was not significant (from 5.1° to 4.3°). Therefore, this suggests that alkali-treatment

can improve the coverage of polymer by tapering and dispersing the SiNWs which is ideal for the infiltration of polymer.

Table 3 Solar cells performance of the hybrid solar cells with different tapered of SiNWs made by immersing in the NaOH solution for 0s, 15s, 30s, 45s and 60s, respectively. All the lengths of SiNWs are 0.45 μm

Alkali-treated time (s)	J_{sc} (mA/cm^2)	V_{oc} (V)	F.F (%)	PCE (%)
0	19.53	0.44	51	4.53
15	23.13	0.47	53	5.76
30	26.66	0.46	54	6.87
45	19.23	0.46	56	4.95
60	14.34	0.45	52	3.42

The J−V curves of the devices under different alkali treatment are shown in Figure 6(a). The key cell parameters including J_{sc}, V_{oc}, FF, PCE are listed in table 3. For a device with alkali treatment, the obvious difference in the J_{sc} data is interesting compared to without alkali treatment, and J_{sc} increased first and then decreased with the increment of alkali treatment time. The maximum J_{sc} of 26.66 mA/cm^2 of a cell which is infiltrated 30 s is obtained, but J_{sc} of cell with 60 s infiltration is the minimum. It indicates that excessive extended time in the alkali treatment will lead to a decrease on junction area between polymer and Si. Therefore, the infiltrated time of 30 s is a proper time for polymer effectively to form a well core-shell structure and provide an efficient pathway for the minority charge carriers transfer/transport. For V_{oc}, the differences are insignificant with different time alkali treatment. V_{oc} was improved from 0.44V to 0.47V compared to no alkali treatment. Generally, [30-33] V_{oc} can be expressed as follow:

$$V_{OC} = \frac{nkT}{q} \ln\left(\frac{J_{SC}}{J_O} + 1\right) \quad (3)$$

where, J_{sc} is the short circuit current density, and J_o, n, k, T, and q are reverse saturation current density, diode ideality factor, Boltzmann constant, absolute temperature, and elementary charge, respectively. The equation indicates that the increase in J_{sc} would lead to an increase in V_{oc}. The result can also be observed from Fig. 6(a). In table 3, TSiNWs/PEDOT: PSS hybrid cell made in this work exhibits a peak PCE of 6.87% with a V_{oc} of 0.46 V and a FF of 54 when SiNWs are immersed in NaOH solution for 30s. The results also confirm that alkali treatment can prompt effectively PEDOT: PSS to fill into the TSiNWs, which can reduce the surface recombination loss and enlarge interface of the Schottky junction between the polymer and SiNWs. Therefore, it is inevitable to improve

the electrical performance of TSiNWs/PEDOT: PSS cells.

To identify the mechanism for increasing the photocurrent in TSiNWs/PEDOT: PSS cells, the dark J-V of cells was also measured in the properties of electrical aspect and shown in Fig .6(b). The value of dark J-V of cells reduces as increasing the time of alkali treatment. This may be interpreted as over time alkali treatment cause the nanowires to became a tubby tapered structure, which can allow the subsequent polymer cover SiNWs uniformly via spin coating and forming well covered core (TSiNWs)-shell (PEDOT: PSS) structure remains seldom defects, And thus possess smaller the dark J-V. However, the effective junction area will be reduced, which go against to more minority charge carriers toward the respective electrode.

Similar to the previous fitting approaches，the value of n corresponding to heterojunction of SiNWs / PEDOT:PSS with alkali treatment for different time was also calculated and shown in table 4. From table 4, one can find that the SiNWs/PEDOT: PSS with 30s alkali treatment possess smaller n and I_s compared to other samples, which indicates PEDOT:PSS layer and TSiNWs forming a well-defined heterojunction interface which can improve carrier transport and the lifetime of minority carrier[37]. Therefore, 30s alkali treatment processing is optimum treatment time for improving the PCE of TSiNWS hybrid solar cells .

Order to analysis optical properties of the hybrid solar cells, the reflectance of TSiNWs and EQE spectra of were also measured. Figure 6 (c) shows the reflectivity of SiNWs substrate as a function of spectra in the range of 300-1000 nm. One can find that the smooth surface (0 s) is easier to reflect light, but the stocky surfaces (45 s, 60 s) are easier to scatter the incident light. Therefore, the nanowires infiltrated time of 30 s is useful for light absorption, which leads to multiple scattering of sunlight, which enhances light trapping and causes much lower reflectance [38]. This result is also embodied in EQE which is shown in Fig. 6(d), where the device based on SiNWs infiltrated in the NaOH solution for 30 s obtains a maximum EQE of 54% compared to the others. The proper surface structure is useful not only for junction area but also for the light reflectivity.

Table 4. The diode ideality factor and the reverse bias saturation current of the hybrid device s with different tapered of SiNWs made by immersing in the NaOH solution for 0s, 15s, 30s, 45s and 60s, respectively. All the lengths of SiNWs are 0.45 μm

Alkali-treated time **(s)**	n	J_s (mA)
0	2.03	6.32×10^{-4}
15	1.94	5.23×10^{-4}
30	1.78	3.45×10^{-4}
45	2.06	7.56×10^{-4}
60	2.41	2.29×10^{-3}

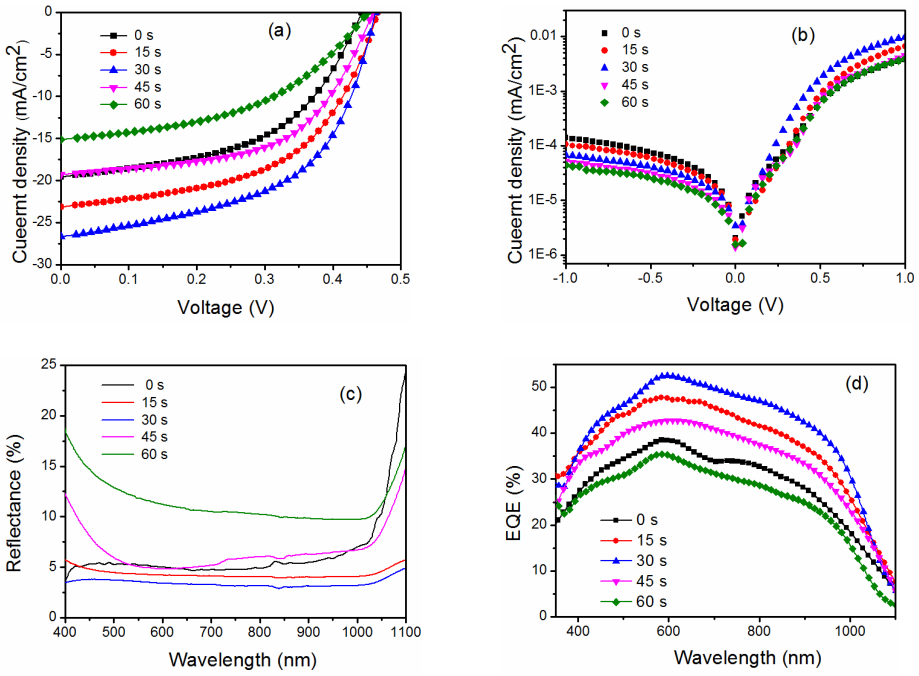

Fig. 6 (a) J–V (b) Dark current density−voltage (J−V) characteristics (c) Reflectance and (d)EQE spectra of hybrid solar cells with TSiNWs at different NaOH treating time for 0s, 15s, 30s, 45s and 60s, respectively, all the lengths of SiNWs are 0.45μm.

Conclusions

A promising hybrid solar cell device based on tapered silicon nanowires arrays and PEDOT: PSS was manufactured and discussed. The results indicate that the morphology and length of SiNWs are indispensable to achieve the highest performance and 30% NaOH solution treatment can effectively tune the morphology of SiNWs, which results in the largest PCE of 6.87% for TSiNWs/PEDOT: PSS hybrid cell with an optimized TSiNWs length of 0.45μm. Therefore, alkali treatment is a simple and effective method to improve performance of SiNWs /PEDOT:PSS hybrid devices, although the open circuit voltage of 0.47 V is relatively low compared to the previous similar reports. However, more concerning, an optimized SiNWs device was not further passivated in our results, and the thin copper film (12 nm thickness), was adopted as anode electrode, not commonly gate electrode, Thus, the performance of the proposed TSiNWs/PEDOT: PSS hybrid solar cell can be further improved by fully optimizing processing.

Acknowledgments

This work is supported by the National Natural Science Foundation of China under grant (No. 11074066) and Henan Provincial Basic and Frontier Project (No.132300410248).

References

1. E. C. Garnett and P. Yang, *Journal of the American Chemical Society*, 2008, **130**, 9224-9225.
2. E. Garnett and P. Yang, *Nano letters*, 2010, **10**, 1082-1087.
3. C.-Y. Liu, Z. C. Holman and U. R. Kortshagen, *Nano letters*, 2008, **9**, 449-452.
4. G. Yuan, H. Zhao, X. Liu, Z. S. Hasanali, Y. Zou, A. Levine and D. Wang, *Angewandte Chemie*, 2009, **121**, 9860-9864.
5. E. Bundgaard and F. C. Krebs, *Solar Energy Materials and Solar Cells*, 2007, **91**, 954-985.
6. S. Jeong, E. C. Garnett, S. Wang, Z. Yu, S. Fan, M. L. Brongersma, M. D. McGehee and Y. Cui, *Nano letters*, 2012, **12**, 2971-2976.
7. X. Li, *Current Opinion in Solid State and Materials Science*, 2012, **16**, 71-81.
8. J.-Y. Chen, C. Con, M.-H. Yu, B. Cui and K. W. Sun, *ACS applied materials & interfaces*, 2013, **5**, 7552-7558.
9. M. Pietsch, M. Y. Bashouti and S. Christiansen, *The Journal of Physical Chemistry C*, 2013, **117**, 9049-9055.
10. J. P. Thomas, L. Zhao, M. Abd-Ellah, N. F. Heinig and K. T. Leung, *Analytical chemistry*, 2013, **85**, 6840-6845.
11. F. Zhang, D. Liu, Y. Zhang, H. Wei, T. Song and B. Sun, *ACS applied materials & interfaces*, 2013, **5**, 4678-4684.
12. C. Y. Kuo and C. Gau, *Applied Physics Letters*, 2009, **95**, 053302.
13. F. Zhang, T. Song and B. Sun, *Nanotechnology*, 2012, **23**, 194006.
14. S. Dayal, M. O. Reese, A. J. Ferguson, D. S. Ginley, G. Rumbles and N. Kopidakis, *Advanced Functional Materials*, 2010, **20**, 2629-2635.
15. I. Khatri, A. Hoshino, F. Watanabe, Q. Liu, R. Ishikawa, K. Ueno and H. Shirai, *Thin Solid Films*, 2014, **558**, 306-310.
16. S. Thiyagu, C.-C. Hsueh, C.-T. Liu, H.-J. Syu, T.-C. Lin and C.-F. Lin, *Nanoscale*, 2014, **6**, 3361-3366.
17. M. Sharma, P. R. Pudasaini, F. Ruiz-Zepeda, D. Elam and A. A. Ayon, *ACS applied materials & interfaces*, 2014, **6**, 4356-4363.
18. L. He, C. Jiang, H. Wang and D. Lai, *Applied Physics Letters*, 2012, **100**, 073503.
19. L. He, C. Jiang, H. Wang and D. Lai, *ACS applied materials & interfaces*, 2012, **4**, 1704-1708.
20. L. M. Chen, Z. Hong, G. Li and Y. Yang, *Advanced Materials*, 2009, **21**, 1434-1449.
21. K. Peng, Y. Xu, Y. Wu, Y. Yan, S. T. Lee and J. Zhu, *small*, 2005, **1**, 1062-1067.
22. Z. Fan, H. Razavi, J.-w. Do, A. Moriwaki, O. Ergen, Y.-L. Chueh, P. W. Leu, J. C. Ho, T. Takahashi and L. A. Reichertz, *Nature materials*, 2009, **8**, 648-653.
23. F. Bai, M. Li, R. Huang, Y. Li, M. Trevor and K. P. Musselman, *RSC Advances*, 2014, **4**, 1794-1798.
24. D. Ginger and N. Greenham, *Physical Review B*, 1999, **59**, 10622.
25. L. E. Greene, M. Law, B. D. Yuhas and P. Yang, *The Journal of Physical Chemistry C*, 2007, **111**, 18451-18456.
26. B. M. Kayes, H. A. Atwater and N. S. Lewis, *Journal of applied physics*, 2005, **97**, 114302.
27. P. Yu, C.-Y. Tsai, J.-K. Chang, C.-C. Lai, P.-H. Chen, Y.-C. Lai, P.-T. Tsai, M.-C. Li, H.-T. Pan and Y.-Y. Huang, *ACS nano*, 2013, **7**, 10780-10787.
28. W.-R. Wei, M.-L. Tsai, S.-T. Ho, S.-H. Tai, C.-R. Ho, S.-H. Tsai, C.-W. Liu, R.-J. Chung and J.-H. He, *Nano letters*, 2013, **13**, 3658-3663.
29. H. J. Syu, S. C. Shiu, Y. Hung Jr, C. C. Hsueh, T. C. Lin, T. Subramani, S. L. Lee and C. F. Lin, *Progress in Photovoltaics: Research and Applications*, 2013, **21**, 1400-1410.
30. Y. Jiang, R. Qing, H. Yang, C. Chen, H. Ma and F. Chang, *Applied Physics A*, 2013, **113**, 13-17.

31. P. R. Pudasaini, F. Ruiz-Zepeda, M. Sharma, D. Elam, A. Ponce and A. A. Ayon, ACS applied materials & interfaces, 2013, 5, 9620-9627.
32. S. Cheung and N. Cheung, Applied Physics Letters, 1986, 49, 85-87.
33. H.-J. Syu, S.-C. Shiu and C.-F. Lin, *Solar energy materials and solar cells*, 2012, **98**, 267-272.
34. W. Lu, C. Wang, W. Yue and L. Chen, *Nanoscale*, 2011, **3**, 3631-3634.
35. A. Merlos, M. Acero, M. Bao, J. Bausells and J. Esteve, *Journal of Micromechanics and Microengineering*, 1992, **2**, 181.
36. C. R. Tellier and A. Charbonnieras, *Sensors and Actuators A: Physical*, 2003, **105**, 62-75.
37. X. Wang, K. Q. Peng, X. J. Pan, X. Chen, Y. Yang, L. Li, X. M. Meng, W. J. Zhang and S. T. Lee, *Angewandte Chemie International Edition*, 2011, **50**, 9861-9865.
38. Y. Jiang, R. Qin, M. Li, G. Wang, H. Ma and F. Chang, *Materials Science in Semiconductor Processing*, 2014, **17**, 81-86.